



# Mechanically Robust Transparent Conducting Electrodes for Flexible Perovskite Solar Cells

Unsoo Kim<sup>1,2</sup> · Jieun Lee<sup>2,3</sup> · Yun Seog Lee<sup>2,3</sup> · Mansoo Choi<sup>2,3</sup> 

Received: 9 August 2024 / Revised: 1 September 2024 / Accepted: 5 September 2024

© The Author(s), under exclusive licence to Korean Institute of Chemical Engineers, Seoul, Korea 2024

## Abstract

Perovskite solar cells (PSCs) offer unique advantage of enabling lightweight and flexible power sources compared to the commercially available rigid wafer-based silicon solar cells, while their power conversion efficiencies are now nearly comparable. To ensure high performance, flexibility and lightweight characteristics in flexible perovskite solar cells and modules, it is essential to develop electrodes that are highly conductive, highly transparent, flexible and thin. In this review, we first highlight important technical metric, figure of merits (FoM), that reflects not only the optical and electrical properties of the transparent electrodes but also their mechanical flexibility. Then, we review recent advancements in transparent conductive electrodes for flexible perovskite solar cells, focusing on various materials and designs including conducting polymers, metal nanowires and meshes, carbon-based nanomaterials, transparent conducting oxides and other novel materials. Lastly, we discuss the challenges and future prospects toward commercialization of flexible perovskite solar modules.

**Keywords** Perovskite solar cells · Flexible transparent conducting electrodes · Flexible optoelectronics · TCE design principle · Mechanical reliability

## Introduction

Hybrid organic–inorganic halide perovskites based solar cells (PSC) have garnered significant attention in the field of photovoltaics due to their remarkable power conversion efficiencies (PCE) and cost-effective production processes [1]. The unique optoelectronic properties of perovskite materials, which include high absorption coefficients [1], tunable bandgaps [2], and long carrier diffusion lengths [3, 4], have enabled PSCs to achieve astonishing efficiencies exceeding 26% in a relatively short period since their inception [5]. Unlike traditional silicon-based solar cells, perovskites can be processed from solution at low temperatures [6–8], allowing

more economic and versatile manufacturing techniques [9]. The advantage of high performance and economic production positions PSCs as one of the most promising candidates for next-generation solar energy harvesting technologies.

With the rising demand for portable, wearable, lightweight, and multi-purpose electronic devices grows, the necessity for flexible energy sources has become increasingly important. Flexible lightweight perovskite solar cells (f-PSCs) address this need by combining the superior optoelectronic properties of the perovskite materials with the mechanical flexibility required for integration into various lightweight thin substrates. This represents a significant advantage over commercially available rigid and relatively heavier silicon solar cells. Several key factors suggest that flexible and lightweight solar cell would be the ideal distinctive application of PSCs: the total device thickness of only 1  $\mu\text{m}$  excluding the substrate, perovskite photoactive layers are compatible with flexible substrates due to their low process temperatures [6], they are suitable for solution-processed roll-to-roll (R2R) manufacturing [10, 11], and they offer the highest power-per-weight ratio among all existing solar cell technologies [12]. Recent advancements have enabled f-PSC to achieve PCE comparable to their rigid counterparts, with values reaching 25.09% (certified

✉ Yun Seog Lee  
leeyunseog@snu.ac.kr

✉ Mansoo Choi  
mchoi@snu.ac.kr

<sup>1</sup> Photovoltaics Research Department, Korea Institute of Energy Research, Daejeon, Republic of Korea

<sup>2</sup> Global Frontier Center for Multiscale Energy Systems, Seoul National University, Seoul, Republic of Korea

<sup>3</sup> Department of Mechanical Engineering, Seoul National University, Seoul, Republic of Korea

24.90%) [13]. Additionally, they have demonstrated superior mechanical durability and flexibility, even with foldable and crumpled flexibility [14, 15]. Previous research has shown applications of f-PSCs as wearable power sources [16, 17], in drones [12], small aerial vehicles [18] and other devices. The ability to install lightweight f-PSCs on curved surfaces, where conventional rigid solar cells are unsuitable, opens up new possibilities for installation in diverse areas including buildings, aerial vehicles, space power sources, and portable power sources [19–25]. This significantly increase overall the portion of renewable energy production and bring us closer to achieving carbon neutrality.

The core device component when transforming rigid PSCs (r-PSCs) into f-PSCs is the transparent conducting electrodes (TCEs). Replacing rigid TCEs (r-TCEs) with flexible TCEs (f-TCEs) requires more than simply switching from a rigid substrate (e.g. glass) to a flexible substrate. The polymer-based substrates typically used in f-TCEs impose limitations on heat treatment temperatures, which can alter the properties of indium-tin-oxide (ITO) coated on the flexible substrates. Additionally, different process conditions must be applied when coating functional layers, including perovskite layer, on top of f-TCEs compared to fabricating rigid perovskite solar cells (r-PSCs). This is due to different physical properties of flexible substrates, such as thermal conductivity and the coefficient of thermal expansion (CTE). Meanwhile, traditional transparent conducting oxide (TCO)-based TCEs used in r-PSCs are highly inflexible, necessitating the use of alternative materials for f-TCEs [17, 26]. Various types of f-TCEs have been successfully fabricated and applied to f-PSCs using novel nanomaterials such as conductive polymers [28–30], metal nanowires and meshes [31–36], graphene [37–40], or emerging nanomaterials [41]. The mechanical and optoelectronic properties of f-TCEs vary significantly depending on the transparent electrode material [42], and numerous considerations must be taken into account during device fabrication with these materials. Understanding the properties and fabrication techniques of these materials is essential, especially since the architecture and structure of the f-TCEs can also impact the performance of f-PSCs [43, 44]. Therefore, comprehending the materials, structures, and fabrication methods of transparent electrodes is crucial.

In this review, we review recent developments of f-TCE substrates, highlighting the properties of f-TCEs based on different materials, examples of their application in f-PSCs, and the standards and engineering perspectives on the key performance metrics of f-TCEs. To achieve high performance, flexibility, and lightweight characteristics, the requirements for sheet resistance ( $R_s$ ), optical transmittance, and power-weight ratio of the final f-PSC product are discussed. We outline the evolution of the FoM as a key indicator of the optoelectronic performance of f-TCEs, along with the mechanical

engineering considerations necessary to ensure the flexibility and mechanical durability of f-PSCs. In addition, we cover fundamental principles and characteristics of conductive polymers, metal nanowires and meshes, carbon allotropes, TCOs, and emerging novel nanomaterials, as well as important considerations when applying these materials to PSCs. Several key examples are highlighted, with a particular emphasis on the material suitability for fabricating large-area perovskite solar modules (PSMs), which is essential for commercialization. Finally, we address the challenges that f-TCEs must overcome to facilitate the commercialization of f-PSCs.

## Performance of f-TCEs

### Optoelectronic Performance of f-TCEs

TCEs are essential components in various optoelectronic devices, including photovoltaics. Their performance is typically evaluated using a FoM that balances two critical physical properties: optical transmittance and sheet resistance of TCEs. Various FoMs have been proposed to quantify the balance between these two critical properties. Here, we briefly review key FoMs, providing a mathematical framework and comparative analysis to understand their application and limitations.

Fraser and Cook (1972) defined a FoM as

$$\phi_{FC} = \frac{T}{R_s},$$

where  $T$  and  $R_s$  denote optical transmittance and sheet resistance, respectively [46]. This FoM is the simplest form, directly relating the two properties of TCE. It suggests that higher transmittance and lower sheet resistance yield a better TCE. Haacke (1976) modified the FoM to

$$\phi_H = \frac{T^{10}}{R_s},$$

placing a stronger emphasis on transmittance, making it more suitable for applications requiring high optical transparency [47]. In 2002, Dressel and Grüner [48] proposed a dimensionless FoM based on the ratio of direct current (DC) conductivity ( $\sigma_{DC}$ ) to optical conductivity ( $\sigma_{OP}$ ):

$$\phi_{DG} = \frac{\sigma_{DC}}{\sigma_{OP}}$$

The  $T$  and optical conductivity are related as:

$$T = \left(1 + \frac{\sigma_{OP} \cdot Z_0}{2}\right)^{-2},$$

where  $Z_0$  is the impedance of free space (377  $\Omega$ ). The DC conductivity and sheet resistance are related by:

$$\sigma_{DC} = \frac{1}{R_s \cdot t}$$

Substituting these into the FoM equation yields:

$$\phi_{DG} = \frac{188.5 \cdot T}{R_s}$$

This FoM emphasizes the balance between electrical and optical properties but can overestimate the value of low  $R_s$  when  $T$  is low. Gamboa et al. [49] adopted

$$\phi_{TC} = \frac{J_{PH}}{R_s},$$

where  $J_{PH}$  is the photocurrent density calculated considering the entire spectral range. This approach accounts for the actual photovoltaic performance rather than a single wavelength transmittance. Contreras et al. [50] used

$$\phi_{TC} = \frac{T}{R_s^n},$$

where  $n$  is incorporated as an adjustable exponent to fine-tune the balance between transmittance and sheet resistance.

Anand et al., (2021) [45] introduced the so-called exact FoM, which is expressed as below:

$$\phi_{exact} = \frac{P_{max}(T, R_s)}{P_{ideal}},$$

where  $P_{max}(T, R_s)$  is the maximum power output considering transmittance and sheet resistance, and  $P_{ideal}$  is the ideal maximum power output based on the Shockley–Queisser limit. This FoM normalizes the TCE's performance by comparing it to the ideal photovoltaic performance when using a TCE with measured transmittance. Thus it provides a comprehensive measure that includes the effects of both optical transmittance and sheet resistance over the full spectral range.

The choice of FoM significantly impacts the assessment of TCEs. Traditional FoMs, such as those proposed by Fraser and Cook or Haacke, are simpler but may not fully capture the performance required for modern applications. Advanced FoMs, especially the exact FoM introduced by Anand et al., provide a more accurate and application-specific evaluation by considering the complete spectral performance and photovoltaic efficiency. Anand et al. assessed the effectiveness of different FoMs by simulating hypothetical TCEs with varying transmittances from 10 to 100% and sheet resistances from 0.1 to 10,000  $\Omega \cdot \text{sq}^{-1}$  (Fig. 1). The contour plots highlight that traditional FoMs exhibit a strong dependency on sheet resistance (Fig. 1 A–C), while advanced FoMs like those proposed by Gamboa and Contreras show a more balanced impact (Fig. 1 D–F).

## Mechanical performance of f-TCEs

Another critical performance aspect of f-TCEs is their flexibility. To design and fabricate f-TCEs and f-PSCs with high flexibility, a mechanical engineering approach is required. Regarding the extent to which they can bend, it is essential to understand the strain applied to each layer in a multilayer thin film. The strain on a layer located at position  $z$  in a multilayer thin film with  $n$  layers, bent with a radius of curvature  $r$ , is given by the following equation:

$$\varepsilon = \frac{z - t_b}{r},$$

where  $t_b$  is the position of mechanical neutral plane, which is described as below:

$$t_b = \frac{\sum_{i=1}^n \bar{E}_i h_i \left[ \left( \sum_{j=1}^n h_j \right) - \frac{h_i}{2} \right]}{\sum_{i=1}^n \bar{E}_i h_i},$$

where  $E_i$  and  $h_i$  (or  $h_j$ ) represent the elastic moduli and thickness of each layer of the substrate, respectively.

For instance, considering that the crack onset strain for ITO, where cracks start to form, is approximately 1.19% [51], it can be deduced that an ITO f-TCE placed on a 125  $\mu\text{m}$ -thick PEN substrate can only be bent to a minimal radius of curvature of around 10 mm. It is noteworthy that the existence of a mechanical neutral plane in a multilayer thin film under bending conditions where the strain is zero. By intentionally positioning the key functional layers of a perovskite solar cell at the vicinity of mechanical neutral plane, the mechanical stability of the devices can be significantly enhanced.

In terms of bending capability, the concept of flexural rigidity is crucial. Flexural rigidity refers to the material's resistance to external stress attempting to bend it. The lower the flexural rigidity, the more easily the material bends under external stress, allowing it to conform more closely to the surface it is placed on. The flexural rigidity is particularly important for wearable electronics, and is expressed as below [52]:

$$D = \frac{Et^3}{12(1 - \nu^2)},$$

where  $D$  is the flexural rigidity,  $E$  is the elastic modulus,  $t$  is the thickness, and  $\nu$  is the Poisson's ratio.

From a device fabrication perspective, another mechanical engineering factor to consider is residual stress. During the fabrication of multilayer devices, thermal treatment is often involved, which inevitably results in residual stress due to the difference in CTEs. The extent of bending

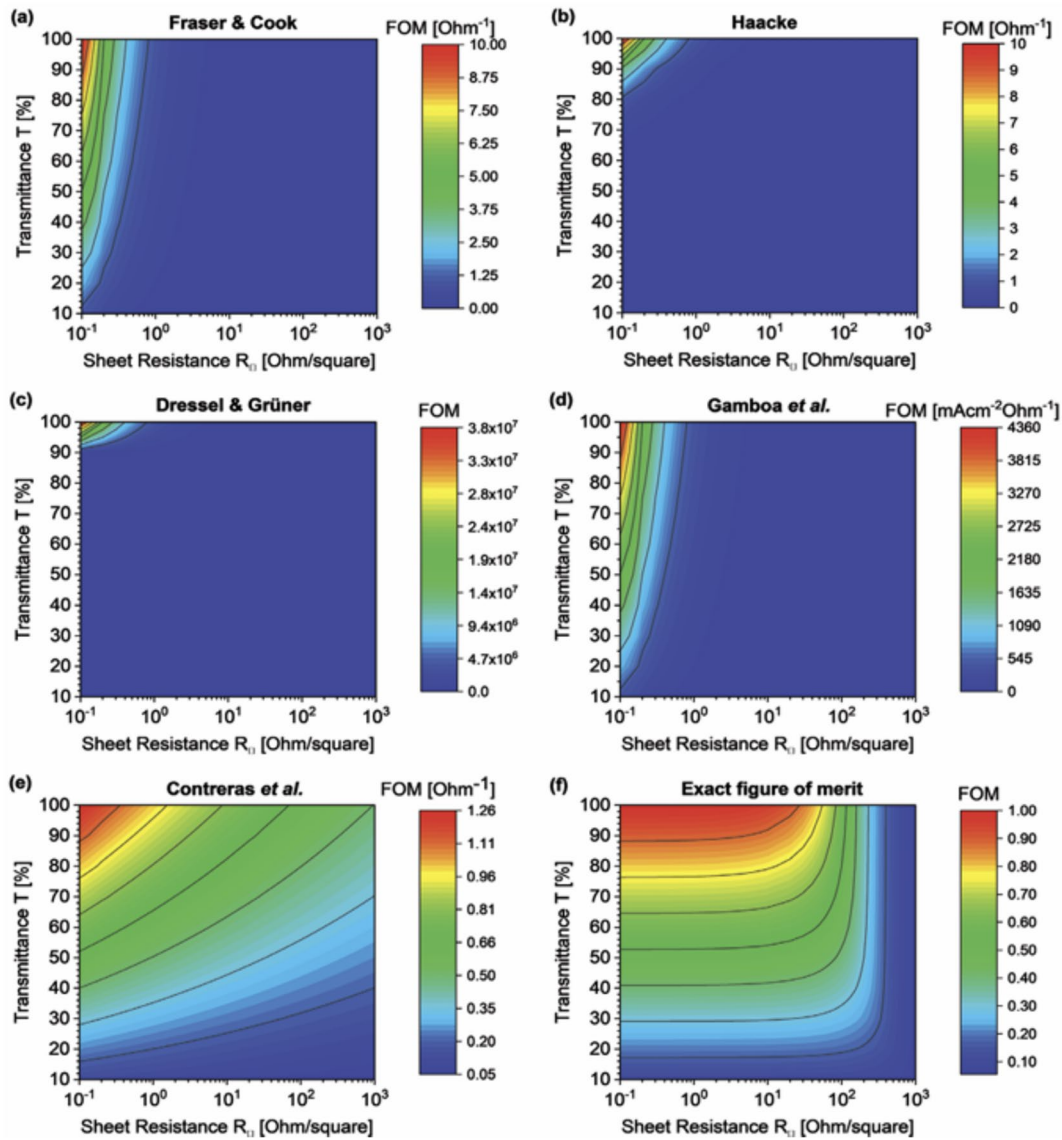


**Fig. 1** Comparison of FoM of TCE for photovoltaic applications. Exact FoM introduced by Anand et al. [45] covers the largest range of transmittance and sheet resistance. Reproduced with permission from [45]. Copyright 2021, John Wiley and Sons

caused by residual stress when a film (*f*) is formed on a substrate (*s*) can be expressed by the Stoney equation:

$$r = \frac{E_s h_s^2}{6(1 - \nu_f) \sigma_f h_f},$$

where *h* is the film thickness,  $\sigma$  is the residual stress. A larger value of *r* indicates a flatter film; thus, maximizing *r* is crucial.

Taking the above equation of flexural rigidity into account, using materials with a smaller thickness and lower elastic modulus is beneficial for enhancing mechanical flexibility in the fabrication of f-TCEs. However, smaller values of these parameters can increase deformation due to residual stress.

Therefore, it is imperative to design and fabricate the device with a comprehensive consideration of all these factors.

The mechanical robustness of f-PSCs is typically demonstrated by their ability to retain their initial PCE after numerous bending cycles. The key test parameters are the radius of curvature and the bending cycles, sometimes bending angle and direction are taken into account.



## f-TCEs for f-PSCs Depending on Materials Type

### Conducting Polymers

Conductive polymers have been considered as promising TCE materials due to their excellent flexibility, while presenting decent optoelectronic properties. The most representative conducting polymer-based TCE material is PEDOT-based compounds. Among them, Poly(3,4-ethylenedioxythiophene):poly(styrene sulfonic acid) (PEDOT:PSS), in particular, has been widely used in various devices such as PSCs, organic photovoltaics (OPVs),

organic light emitting diodes (OLEDs), and photodetectors due to its superior optoelectronic properties and flexibility.

One of the primary challenges with using PEDOT:PSS in PSCs is its chemical stability. The acidic nature of PSS decomposes the perovskite layer when PSS and perovskite layers are in contact. Therefore, developing techniques to prevent the acidic PSS from contacting the perovskite layer is essential when utilizing PEDOT:PSS in PSCs. For instance, some studies have used a compact NiO<sub>x</sub> layer as a hole transport layer (HTL) [53], or deposited a thin-film like LiF layer between perovskite and PEDOT:PSS [54] to prevent the direct contact between PSS and the perovskite layer and ensure stable device operation (Fig. 2A). However, even with these buffer layers, there have been reports of

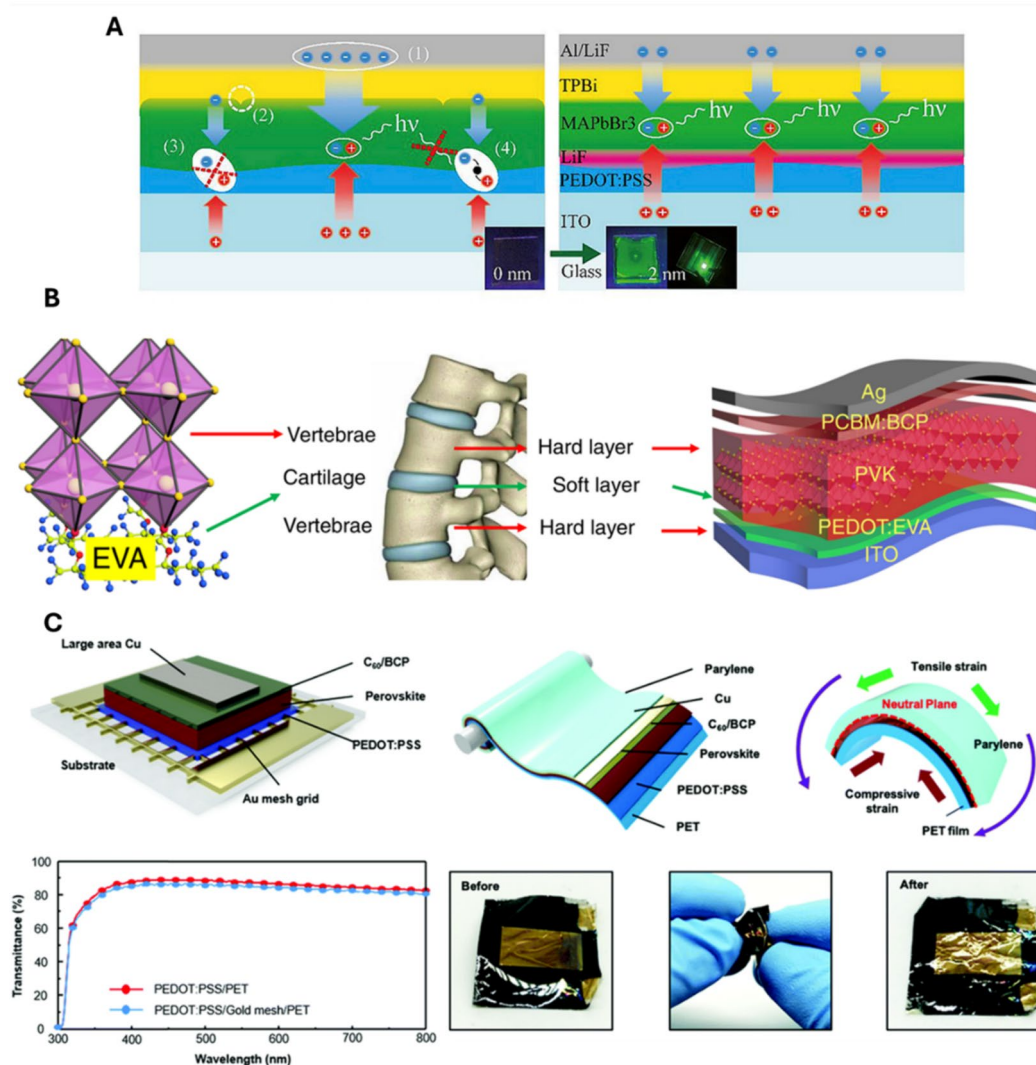


**Fig. 2** Conductive polymer-based f-TCEs for PSCs. **A** Direct contact between perovskite photoactive layer and acidic PEDOT:PSS has been prevented using LiF interlayer. Reproduced with permission from [54]. Copyright 2020, Elsevier. **B** Acidic PSS chain has been replaced by neutral EVA to prevent decomposition of perovskite layer.

Reproduced with permission from [56] Copyright 2020, Springer Nature. **C** PSCs using highly-conductive PEDOT:PSS-Au mesh hybrid f-TCE with neutral plane engineering show crumpling-durable flexibility. Reproduced with permission from [15]. Copyright 2019, The Royal Society of Chemistry

perovskite layer degradation when using PEDOT:PSS [55]. This issue is exacerbated under mechanical deformation of f-PSCs, suggesting that buffer layers may not provide a fundamental solution.

An alternative approach to using buffer layers is to replace the PSS with a material that does not degrade the perovskite. Meng et al., for example, replaced the PSS with ethylenevinylacetate (EVA) in the PEDOT:PSS used as a HTL in f-PSCs (Fig. 2B) [56]. EVA, being neutral in pH, did not degrade the perovskite layer upon direct contact and even enhanced hydrophobicity compared to PSS, promoting larger grain growth in the perovskite crystals. Consequently, f-PSCs fabricated with PEDOT:EVA achieved a higher PCE of 19.87%, excellent mechanical durability (retaining 85% of initial efficiency after 7,000 cycles of bending tests with a 3 mm radius of curvature), and high chemical stability (retaining 85% of the original efficiency after 3000 h of storage).

Another significant challenge for conductive polymer-based TCEs is their high sheet resistance. For the commercialization of PSCs, large-area scalability is crucial, necessitating TCEs with low sheet resistance as well as having high FoM [57]. Pristine PEDOT:PSS exhibits relatively high sheet resistance, ranging from 200 to 1000  $\Omega\cdot\text{sq}^{-1}$  approximately [58]. With such sheet resistance, perovskite solar cell modules with subcell widths of 5 mm would experience about a resistive power loss of 40%. In various field of optoelectronics, numerous studies have focused on reducing the sheet resistance of PEDOT:PSS. Various types of materials including organic solvents such as ethyleneglycol (EG) and dimethylsulfoxide (DMSO) [59–61], acidic dopants [62–64], and ionic liquids [65, 66] have been applied, resulting in extremely high conductivity of 5012  $\text{S}\cdot\text{cm}^{-1}$  [60]. Lee et al. [15] developed a hybrid flexible TCE by introducing an Au mesh into PEDOT:PSS (Fig. 2C). The incorporation of the Au mesh significantly reduced the sheet resistance with negligible loss in transmittance, resulting in f-PSCs based on PEDOT:PSS/Au-mesh with a PCE of 17.03% for a 0.0780  $\text{cm}^2$ -sized device and 13.6% for a 1.2  $\text{cm}^2$ -sized device. Notably, combining high conductivity from Au mesh and high flexibility from PEDOT:PSS, these devices maintained their efficiency after 10,000 bending cycles at a 0.5 mm radius of curvature and retained over 88% of their initial efficiency after 100 crumpling cycles, showcasing excellent mechanical durability, which was accompanied with mechanical neutral plane engineering using protective parylene-C capping layer.

Despite some studies demonstrating PEDOT:PSS based f-TCEs with excellent FoM and very low sheet resistance [59, 64, 65], there are few instances where these f-TCEs have been used to fabricate high-efficiency large-area PSMs. The fabrication of PSMs typically involves laser processing; however, conductive polymers are reported to degrade

due to heat generated during this process, owing to their low thermal stability. Consequently, high-efficiency PSMs based on PEDOT:PSS have primarily employed mechanical or chemical etching methods rather than laser processing, indicating the need for additional research to address these challenges [53, 56].

## Metal Nanowires (nanowires) and Meshes

To harness the high conductivity of metals while maintaining optical transparency, metal nanowires and metal mesh structures can be employed as transparent electrodes. These metal meshes and nanowires not only exhibit excellent optoelectronic properties but also provide high mechanical durability due to the ductile nature of metals. With the appropriate materials and fabrication processes, high-performance f-TCEs can be fabricated at a very low cost. For instance, Song et al. demonstrated highly conductive ( $R_s \sim 7.9 \Omega\cdot\text{sq}^{-1}$ ) and transparent (300–900 nm average transmittance  $\sim 85\%$ ) Ag-mesh based f-TCEs via self-assembled bubble template technique [36] (Fig. 3A), and even higher conductivity ( $R_s \sim 0.2\text{--}0.5 \Omega\cdot\text{sq}^{-1}$ ) and transmittance ( $\sim 85\%\text{--}87\%$ ) has been demonstrated with Ni-mesh-based f-TCE fabricated through simple and cost-effective nanoimprinting method [34] (Fig. 3B).

Metal nanowires and meshes share similar characteristics and performance as electrodes but differ in several key aspects. One significant difference is that metal meshes offer more design flexibility. Parameters such as mesh width, spacing, shape, and thickness can be adjusted to engineer the optoelectronic properties, which allows for more ordered and controlled fabrication. Unlike metal nanowires, metal meshes can be made thicker through various fabrication methods. Increasing the thickness of the mesh can significantly reduce sheet resistance without substantially affecting light transmission, thereby enhancing the FoM of f-TCEs. For example, Galagan et al. systematically studied the effect of mesh thickness on optoelectronic property of inkjet-printed Ag grid TCEs by controlling the processing parameters, revealing the beneficial aspect of higher thickness of metal meshes [67] (Fig. 3C).

However, there are limitations to increasing the height of the mesh. PSCs are typically fabricated by coating functional layers onto TCEs, and incorporating high-aspect-ratio metal meshes into TCEs can lead to significant surface roughness, preventing uniform coating of the perovskite and charge transport layers (CTL). To address this issue, a technique has been developed to embed metal meshes within the substrate, effectively flattening the surface of f-TCEs. For instances, 40-nm-thick Ni meshes were successfully embedded in polyethylene terephthalate (PET) substrate [34, 36], and even thicker Ag meshes of 600 [35] and 700 nm [68] were embedded in

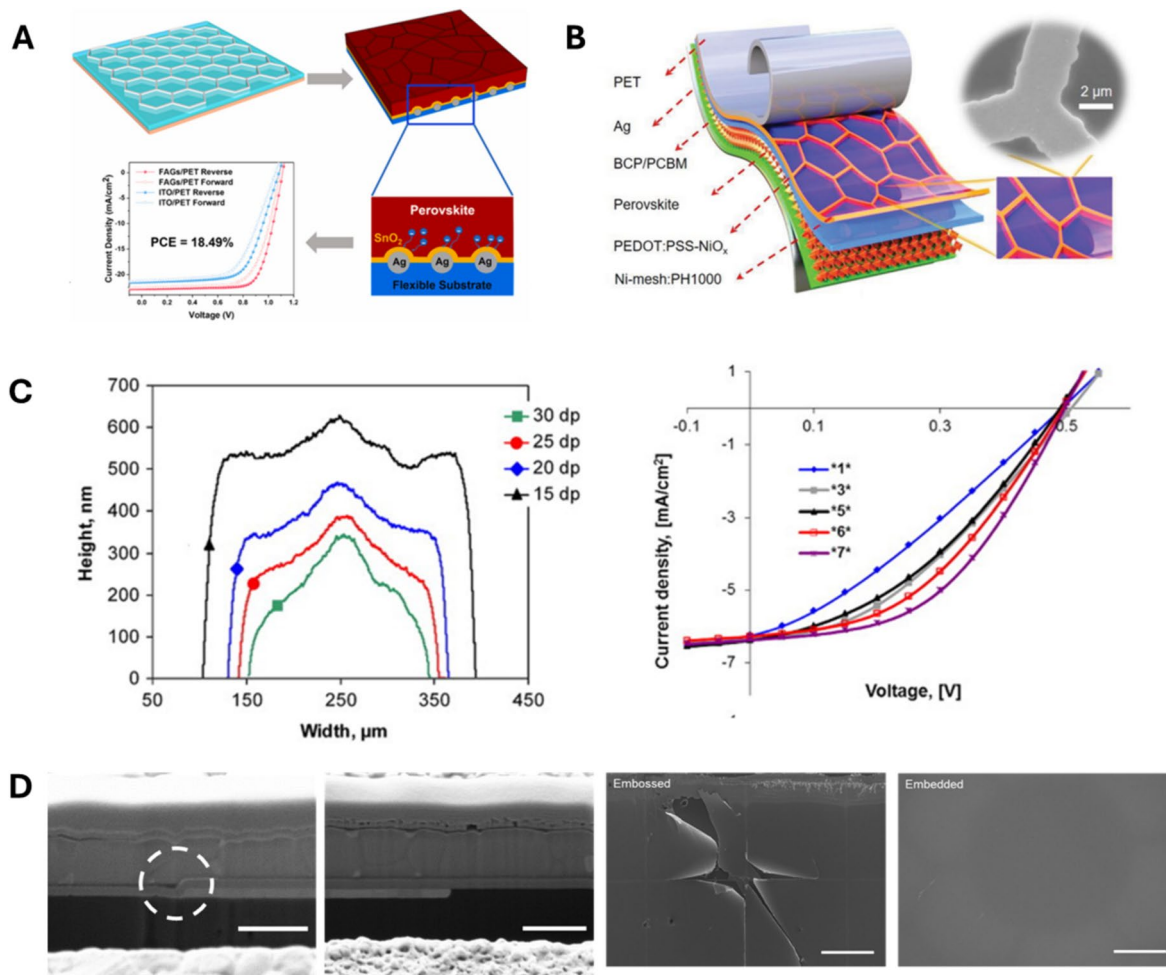


**Fig. 3** Metal mesh and NW based f-TCEs for PSCs. f-TCEs and f-PSCs using metal meshes produced with cost-effective fabrication processes such as **A** nanoimprinting and **B** template methods. **A** Reproduced with permission from [36]. Copyright 2021, Elsevier. **B** Reproduced with permission from [34]. Copyright 2020, John Wiley and Sons. **C** Effect of height of metal meshes on performance of

TCEs and solar cells. Reproduced with permission from [67]. Copyright 2012, Elsevier. **D** Comparison of influence of embedded and non-embedded (embossed) metal mesh on photovoltaic and mechanical performance of f-PSCs. Reproduced with permission from [14]. Copyright 2022, John Wiley and Sons

ultraviolet (UV)-curable resin attached to PET substrates (Fig. 3C). This produced remarkable optoelectronic properties ( $R_S \sim 0.2\text{--}0.5 \Omega\cdot\text{sq}^{-1}$  and  $T \sim 85\%\text{--}87\%$  for Ni mesh,  $R_S \sim 7.05$  and  $1.67 \Omega\cdot\text{sq}^{-1}$  and  $T \sim 87.2\%$  and  $88.6\%$  for 600- and 700 nm-thick Ag mesh, respectively). Kim et al. systematically compared the effects of embedded and non-embedded (embossed) Au meshes on PCE and mechanical durability of f-PSCs against bending [14]. Embedding the metal mesh significantly reduced non-radiative recombination due to incomplete coating and improved mechanical durability by eliminating structures that induces stress concentration on the perovskite layer (Fig. 3D). Combining advantages of embedding metal meshes within substrate mentioned above and the fact that embedding mesh also has potential to produce extremely conductive f-TCEs by further increasing the embedded mesh thickness,

embedded-mesh type f-TCEs are among the most promising forms of f-TCEs.

Meanwhile, neither metal nanowires nor meshes can be solely used as f-TCEs for perovskite solar cells. Non-noble metals used in these structures such as Ag, Cu, and Ni can react with the perovskite material, adversely affecting the performance and stability of the solar cells. Additionally, most materials used as CTLs in perovskite solar cells often exhibit low conductivity, which hinders efficient lateral charge transport and charge collection at the mesh or nanowire electrodes. Therefore, other transparent electrode materials such as conducting polymers, graphene, and TCOs are often used as buffer layers in conjunction with metal nanowires or meshes, forming hybrid-material type f-TCEs. Most of the previous works cited above adopt buffer electrode materials, with only a few exceptions [31, 69, 70].



## Carbon-Based Materials

Carbon allotrope-based transparent electrodes represent another promising class of f-TCE materials. Notably, graphene and carbon nanotubes (CNTs) exhibit exceptional optical transparency and conductivity, making them attractive candidates for transparent electrodes. Graphene, for instance, can theoretically achieve a conductivity of  $10^6$  S·cm<sup>-1</sup> and single-layer graphene (SLG) can have an optical transparency of over 95% [71, 72]. CNTs can theoretically reach conductivities of  $10^4$ – $10^5$  S·cm<sup>-1</sup> with over 90% transparency [71, 73]. Moreover, graphene boasts a theoretical tensile strength of up to 1 TPa [74], while CNTs can exceed 100 GPa [75], making both materials highly suitable for flexible transparent electrodes.

High-quality graphene can be obtained through chemical vapor deposition (CVD) on metal thin films, typically Ni or Cu, and its optoelectronic and mechanical properties can be adjusted based on the number of graphene layers. CNTs are classified into single-walled (SWNT), double-walled (DWNT), and multi-walled (MWNT) types, depending on the number of concentric tubes, with SWNTs and DWNTs commonly used as transparent electrodes. Additionally, CNTs can be metallic, semiconducting, or insulating based on their chirality.

Despite of their theoretically excellent electrical conductivities, the actual conductivities of fabricated graphene and CNTs fall significantly short of these theoretical values. CVD-grown graphene contains numerous grain boundaries that degrade its electrical properties, and it is nearly impossible to selectively produce only metallic CNTs. As a result,

the reported sheet resistances for graphene and CNTs range from tens to hundreds of  $\Omega$ ·sq.<sup>-1</sup>. Another issue related to graphene and CNT based f-TCEs is that as graphene and CNTs are primarily fabricated through CVD processes on specific substrates. To produce f-TCEs with these materials, it is crucial to develop transfer techniques that do not damage the graphene and CNTs while transferring them onto flexible substrates. Furthermore, since graphene and CNTs are hydrophobic, surface modification might be necessary to coat some functional layers in PSCs.

Jeon et al. utilized chemical doping methods to increase the conductivity of CNTs. By applying HNO<sub>3</sub> to enhance the conductivity of SWNTs, they reduced the sheet resistance from 208.2 to 23.7  $\Omega$ ·sq.<sup>-1</sup> (Fig. 4A) [76]. Additionally, to improve the conductivity of solution-processable DWNTs, they applied trifluoromethanesulfonic (TFMS) acid, reducing the sheet resistance by 42.1% (Fig. 4B) [77]. Using the doped SWNTs and DWNTs, they fabricated PSCs with efficiencies of 15.3% and 17.2%, respectively. Meanwhile, the Im group used AuCl<sub>3</sub> as a dopant for graphene to increase adhesion and used a 3-aminopropyl triethoxysilane (APTES) interlayer to reduce the sheet resistance, resulting in f-PSCs with a high efficiency of 17.9% [78] (Fig. 4C).

Jeon group adopted an embedding transfer method on colorless-polyimide (cPI) and parylene-C substrates for SWNTs and DWNTs, respectively (Fig. 5A, B) [55, 79]. This method produced ultra-thin f-TCEs with thicknesses within 10  $\mu$ m without damaging the CNTs and provided additional benefits, such as reducing the sheet resistance of SWNTs and removing surface impurities from DWNTs. As a result, they fabricated f-PSCs with very high PCEs of 15.2%

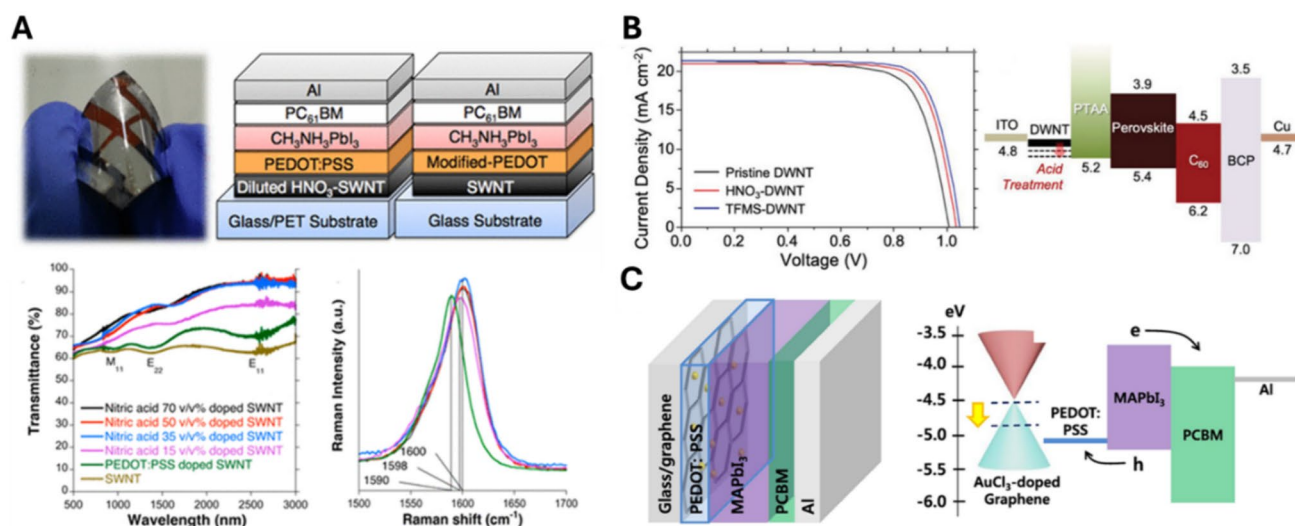


**Fig. 4** Carbon allotrope based f-TCEs for PSCs. Chemical doping strategies to increase conductivities of **A** SWNT with HNO<sub>3</sub>, **B** graphene with AuCl<sub>3</sub> and APTES, and **C** DWNT with TFMS. **A** Reproduced with permission from [76]. Copyright 2015, American Chemi-

cal Society. **B** Reproduced with permission from [77]. Copyright 2019, John Wiley and Sons. **C** Reproduced with permission from [78]. Copyright 2017, Elsevier



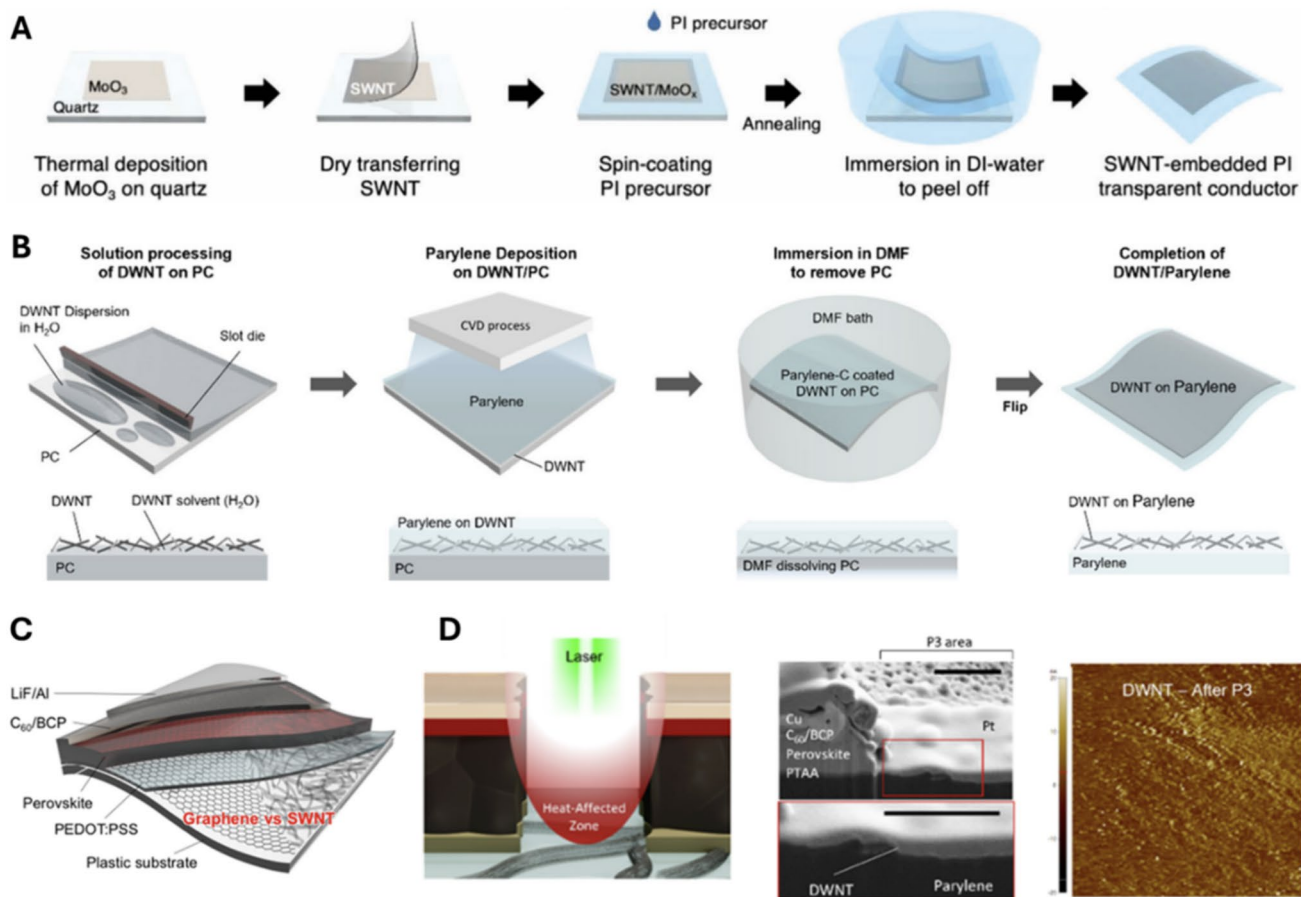


**Fig. 5** Transfer techniques to fabricated CNT based f-TCEs where (A) SWNT is embedded in cPI substrate and (B) DWNT is embedded in CVD-processed parylene-C substrate. **A** Reproduced with permission from [79]. Copyright 2021, John Wiley and Sons. **C** Direct comparison between SWNT and graphene as f-TCE materials for PSCs.

Reprinted with permission from [81]. Copyright 2017, American Chemical Society. **D** Laser scribing process on DWNT-based PSM. Thermally stable DWNT electrodes remained intact even after harsh P3 laser scribing. **B, D** Reproduced with permission from [55]. Copyright 2024, John Wiley and Sons

and 18.1% using SWNT/cPI and DWNT/parylene-C f-TCEs, respectively. In the case of graphene, transfer is typically performed using polymethylmethacrylate (PMMA), and it can also be utilized as a transparent electrode in superstrate-type f-PSCs through transfer methods using PDMS [80].

For surface modification, Yoon et al. successfully coated hydrophilic PEDOT:PSS HTL on the hydrophobic graphene surface by depositing  $\text{MoO}_x$ , which acted as both a surface modification agent and chemical dopant [39]. Xu et al. created active sites on the graphene surface by applying ethylene glycol (EG), enabling the successful formation of an ALD-ZnO ETL on graphene. This modification led to a performance enhancement by 133.9% compared to that of PSCs using non-EG treated graphene [40].

It is noteworthy that Jeon et al. directly compared graphene and CNTs as transparent electrodes for f-PSCs (Fig. 5C) [81]. Graphene f-TCE-based PSCs demonstrated higher PCE due to superior surface morphology and higher transparency, resulting in higher open-circuit voltage ( $V_{OC}$ )

and short-circuit current density ( $J_{SC}$ ). However, CNTs exhibited superior mechanical durability. The study suggested that CNTs could be more commercially viable than graphene if combined with effective doping strategies and coating techniques to control surface roughness.

Studies have explored the fabrication of PSMs using carbon-based f-TCEs. Kim et al. fabricated PSCs using solution-processed DWNT f-TCEs and further developed PSMs using laser scribing (Fig. 5D) [55]. Despite the high sheet resistance of DWNTs ( $\sim 280 \Omega \cdot \text{sq}^{-1}$ ), which resulted in a low PCE of approximately 3.3%, the DWNT-based modules were operational. In contrast, PSMs made with PEDOT:PSS f-TCEs failed to operate due to the vaporization of PEDOT:PSS during the P3 laser scribing process, which disrupted the subcell connections. DWNTs demonstrated higher thermal stability than PEDOT:PSS, withstanding the produced heat during the process without vaporizing (Fig. 5D). This thermal stability suggests that carbon-based transparent electrodes can be more suitable for f-PSC

commercialization, given their comparable optoelectronic and mechanical properties to conductive polymer-based transparent electrodes. However, the high production costs of graphene and CNTs due to current fabrication methods remain a significant barrier. Future advancements should focus on developing cost-effective techniques for producing graphene and CNT-based f-TCEs to enhance their commercial viability.

## Transparent Conducting Oxides

Transparent conducting oxides are the fundamental transparent electrodes for perovskite solar cells and have been primarily used to fabricate high-efficiency PSCs due to their superior optoelectronic properties. Consequently, TCO-based f-TCEs have also been utilized to achieve the highest performance in flexible perovskite solar cells (f-PSCs). The most representative TCO materials include ITO, indium-doped zinc oxide (IZO), and aluminium-doped zinc oxide (AZO), which have been frequently used as transparent electrodes for f-PSCs due to their excellent optoelectronic properties and high flexibility [82]. Record efficiencies have been achieved using TCO-based f-TCEs. Two most popular strategies for achieving high-efficiency f-PSCs are developing efficient charge transport layers with an improved interface quality with perovskite layer [13, 83–85], and incorporating additives that simultaneously enhance efficiency and mechanical characteristics [86–89], which is outside of scope of this review. In PSM

fabrication, TCOs are also the best option in obtaining highest efficiency, enabling the production of a flexible PSM with an efficiency of 18.71% with a device area of 36.50 cm<sup>2</sup> [85].

Although TCOs are the optimal choice in terms of solar cell performance, their major drawback is their low flexibility. TCOs are inherently brittle, and since their thin-film forms are typically deposited via sputtering technique, often requiring substrates thicker than 100 μm to withstand the residual stress caused by heat generated during the process. This makes achieving high flexibility very challenging. Therefore, it is crucial to utilize the excellent optoelectronic properties of TCOs while ensuring high flexibility.

Kim et al. developed a mechanically engineered ITO-based f-TCE that maintains high flexibility while leveraging the superior optoelectronic properties of TCOs (Fig. 6A) [14]. To drastically reduce the stress applied to ITO, they introduced an ultrathin (~10 μm) substrate and further incorporated AlO<sub>x</sub> with a high elastic modulus into the substrate. This approach minimized the warping of the substrate caused by the processing heat during ITO sputtering. Consequently, they developed an f-TCE with superior optoelectronic properties compared to commercial ITO-based f-TCEs, maintaining conductivity even after 10,000 bending cycles at a radius of curvature of 0.5 mm. Based on this f-TCE, they fabricated highly flexible f-PSCs and flexible PSMs with high efficiency (19.16% for small device and 13.16% for PSMs) and foldable flexibility, retaining its initial efficiency after 10,000 cycles of bending test under

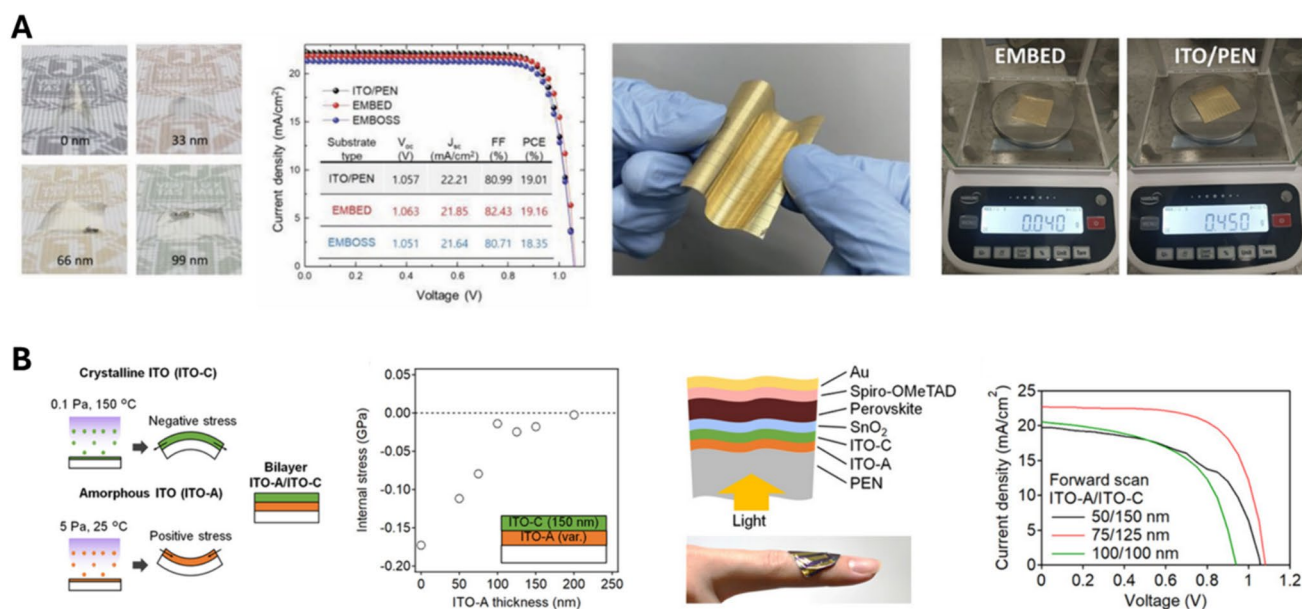


**Fig. 6** TCO based f-TCE for PSCs achieving both high efficiency and excellent mechanical flexibility. **A** Mechanically-engineered ultrathin ITO f-TCE PSCs and PSMs possessing high efficiency, foldable flexibility, and lightweight feature. Reproduced with permission from

[14]. Copyright 2022, John Wiley and Sons. **B** Process-engineered double-layer ITO f-TCE with ultrathin flexible substrate, showing high efficiency and mechanical durability. Reproduced with permission from [90]. Copyright 2023, John Wiley and Sons

0.5 and 1.0 mm of bending radius for PSCs and PSMs, respectively.

Ohashi et al. also aimed to develop highly flexible and high-performance ITO-based transparent electrodes by introducing an ultrathin substrate (Fig. 6B) [90]. To address the warping caused by residual stress during ITO sputtering, they adjusted the sputtering conditions to simultaneously apply both positive and negative residual stress through different ITO layers. This approach led to the development of an ultrathin, highly flexible ITO transparent electrode. Using this electrode, they fabricated perovskite solar cells with an efficiency of 18.2%, maintaining their initial efficiency even after 1,200 bending cycles at a radius of curvature of 1 mm.

## Novel Materials

In addition to the aforementioned TCE materials, new classes of materials are being explored as transparent electrode materials for f-PSCs. While extensive research has not yet been conducted on these materials, several intriguing candidates are worth introducing.

MXenes, a class of two-dimensional (2D) materials composed of transition metal carbides, nitrides, or carbonitrides, exhibit exceptional properties making them ideal for f-TCE material in optoelectronic devices. MXenes demonstrate significant advantages including low sheet resistance and excellent mechanical flexibility. For instance, Zhou et al. demonstrated  $\text{Ti}_3\text{C}_2\text{T}_x$  MXene-based f-TCE for perovskite light-emitting diodes (PLED), which achieved a sheet resistance of  $97.4 \Omega\text{-sq.}^{-1}$  while maintaining high transparency, and show negligible changes in electrical properties even after 5000 bending cycles under bending radius of 1 mm

[91, 92]. Chen et al., also developed a hybrid f-TCE combining Ag NW and 2D MXenes platelets, which was applied to f-PSCs and resulted in remarkable PCE of 20.22% [41]. Furthermore, the hydrophilic surfaces of MXenes allow for uniform dispersion in polar solvents, facilitating cost-effective, large-scale production and aqueous solution processing without surfactants or binders. These properties, combined with their metallic conductivity and ability to be processed in solution, enable MXenes to overcome limitations associated with other transparent conductive materials like CNTs, graphene, and conducting polymers.

Another novel group of f-TCE worth to be introduced is bio-originated f-TCE group. Despite this group actually uses various TCE materials presented above, the novelty lies in their materials used as flexible substrate. Cellulose-based materials such as paper, bamboo, or fabrics such as silk were successfully introduced as flexible substrate of PSCs [16, 93–96]. Bio-compatibility is the most prominent merit of these materials, enhancing eco-friendliness of PSCs and PSCs' potential as wearable power sources. Zhu et al. employed bamboo-derived cellulose fabric as flexible substrate, and successfully fabricated highly flexible (retained 70% of initial efficiency after 1,000 bending cycles at 4 mm bending radius) and efficient (PCE of 11.68%) f-PSCs, which can be bio-degraded with minimal pollutants whereas petroleum-based PET substrates leave toxic residues [16] (Fig. 7A). A f-TCE using silk-derived flexible substrate was demonstrated by Ma et al.. Various shapes such as waves, spirals, bowknots, and even paper crane were successfully made using silk-based f-TCEs, showcasing its superior malleability and pliability, as well as decent solar cell efficiency (PCE of 10.40%) [96] (Fig. 7B).

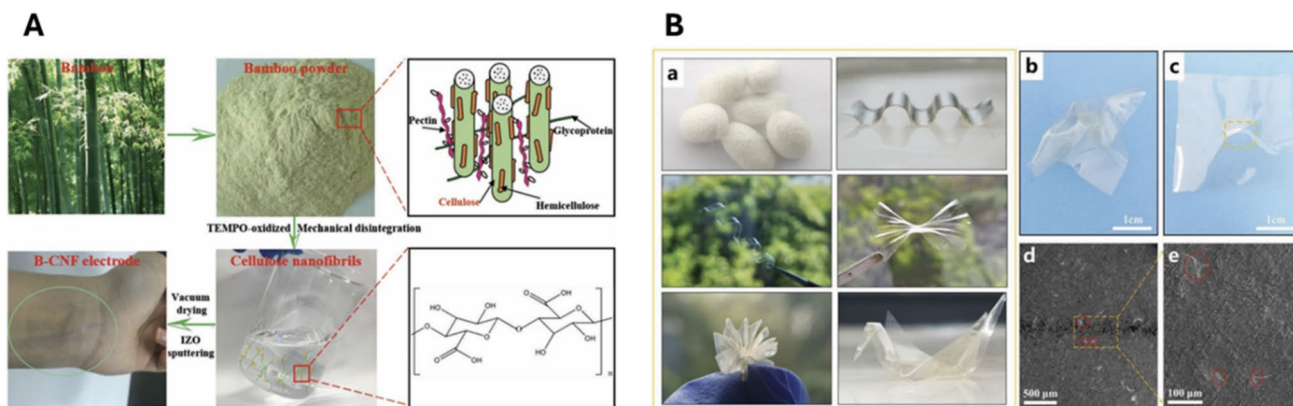


**Fig. 7** Novel nanomaterials and types of f-TCEs for PSCs. **A** Bamboo-derived paper-based f-TCE and **B** silk-derived f-TCE for highly flexible and malleable perovskite solar cells. **A** Reproduced with per-

mission from [16]. Copyright 2019, John Wiley and Sons. **B** Reproduced with permission from [96]. Copyright 2020, John Wiley and Sons



## Challenges and Future Prospect toward Commercialization

### Extremely High Conductivity

As previously discussed, for the commercialization of PSCs, it is essential to scale up their production. Most thin-film solar cell technologies, including PSCs, utilize transparent electrodes, which inherently involve a trade-off between transparency and conductivity, limiting performance enhancement. TCOs have a relatively low sheet resistance of around  $10 \Omega\text{-sq.}^{-1}$ , but this is still significantly higher than that of metals, leading to inevitable resistive losses when charges are collected through the TCEs. As the area of the solar cell increases, these resistive losses scale proportionally, negatively impacting the fill factor of the device.

To address this issue, PSCs are modularized using a monolithic module design to minimize resistive losses caused by the low conductivity of TCEs. However, this modularization creates inactive areas that do not contribute to power generation and requires very precise processing conditions, making it challenging to optimize. Additionally, the laser used for module fabrication can damage the functional layers and the scribed areas, allowing potential degradation sources such as moisture and oxygen to infiltrate, thereby compromising the stability of the PSCs.

Due to these challenges, it is highly desirable to produce modularization-free large-area PSCs, which requires TCEs with extremely high conductivity. A notable example is the finger and busbar type TCEs used in silicon solar cells. Mimicking this approach, adopting metal mesh-based transparent electrodes could enable the production of modularization-free large-area PSCs. Li et al. developed hybrid electrodes by embedding metal meshes in ITO, and they have fabricated high-efficiency (PCE of 22.5%) PSCs with an area exceeding  $100 \text{ mm}^2$  without modularization [97]. To achieve high transmittance and high conductivity in such TCEs, technology for fabricating high aspect ratio metal meshes must be developed. These meshes should be embedded in the substrate to prevent for it to hinder the coating of various functional layers of the PSCs as previously discussed in Sect. “Carbon Based Materials”. To fabricate high aspect ratio metal meshes, alternative techniques to conventional photolithography with thermal evaporation, such as aerosol printing [98–100] or electroplating [101], can be employed. In case of superstrate design where TCEs are formed on the device stack, printing techniques to form high aspect ratio metal mesh on PSCs cell stack without damaging underlying layers are required.

## Environmental Stability: Flexible Encapsulation Technologies

Long-term stability is one of the critical challenges for the commercialization of f-PSCs. Durability against external factors such as heat and moisture is essential for all types of solar cells, and achieving this requires the development of effective encapsulation technologies. While conventional r-PSCs can be encapsulated using glass lids and epoxy resins, these methods are not suitable for f-PSCs. Therefore, flexible encapsulation methods are necessary for flexible solar cells. For flexible encapsulation at the top side of f-PSCs, barrier foil encapsulation can be employed. This method is similar to glass lid encapsulation and utilizes barrier foil and sealants. Commonly used barrier foils include ultra-thin glass thinner than  $50 \mu\text{m}$ , graphene, metal foils, and polymer nanocomposites. Polymer nanocomposites, which incorporate various nanoparticles such as  $\text{Al}_2\text{O}_3$ , ZnO, and graphene into the polymer matrix, are used to enhance the moisture and oxygen barrier properties of the polymer. Unlike r-PSCs, the substrates used for f-PSCs are permeable to moisture and oxygen, necessitating the encapsulation of the substrate as well. Thin film encapsulation (TFE) technology can be applied for this purpose. TFE involves depositing organic or inorganic thin films on flexible substrates like PET and PEN to improve barrier properties while exhibiting excellent flexibility due to their thin thickness (up to several hundreds of nm). Thin films for TFE are typically deposited using processes such as chemical vapor deposition (CVD), atomic layer deposition (ALD), and sputtering. Among them, ALD is capable of forming pinhole-free thin films and is used to deposit various inorganic layers such as  $\text{Al}_2\text{O}_3$ ,  $\text{ZrO}_x$ ,  $\text{TiO}_x$ , and  $\text{HfO}_x$ .

The most common approach involves alternately stacking organic and inorganic layers to create a multilayer (or multidyad) structure. In this structure, inorganic layers primarily serve as moisture and oxygen barriers, while organic layers help alleviate interfacial stress, enhance flexibility, and increase the penetration length of external invasive agents.

### Cost-Effective Production Technologies

Large-scale production of f-TCEs should also be guaranteed for the commercialization of f-PSCs. The manufacturing process for f-TCEs must be cost-effective and scalable. In the case of PSCs, most functional layers can be fabricated using solution processes, and since the annealing temperature is not high, R2R application is feasible. Currently, commercial f-TCEs-based on TCO are produced using R2R methods, however, for the mass production of f-TCEs based on other f-TCE materials, it is necessary to develop large-area R2R coating or printing technologies for these materials.



Jung et al. reported that a R2R process, which employs the Mayer rod coating method, enables the fabrication of Ag-nanowire electrodes embedded in a PET film. These electrodes exhibit a sheet resistance of  $5 \Omega\text{-sq.}^{-1}$  and a transmittance of 85%. [102] (Fig. 8A) Deng et al. demonstrated another R2R process for producing graphene and Ag-nanowire hybrid films via CVD and hot lamination. This approach results in metal Ag-nanowire electrodes fully encapsulated by a large-area monolayer graphene film and a flexible transparent plastic substrate, achieving a sheet resistance of approximately  $8 \Omega\text{-sq.}^{-1}$  and a transmittance of 94%. [103] (Fig. 8B) Lin et al. developed an R2R process for fabricating Ag-nanowire network electrodes, incorporating blow spinning and simultaneous UV irradiation. These electrodes exhibit a sheet resistance of around  $12 \Omega\text{-sq.}^{-1}$  and a transmittance of 95%. [104] (Fig. 8C) Zhong et al. employed an R2R continuous reverse-offset printing process to fabricate metal mesh electrodes using Ag NP ink via slot-die coating, resulting in electrodes with a sheet resistance of  $9.86 \Omega\text{-sq.}^{-1}$  and a transmittance of 90%. [105] (Fig. 8D).

Promising coating technologies for large-scale substrates include spray coating, slot-die coating, and dip coating. For printing of patterned design, gravure printing, flexo printing, inkjet printing, and nanoimprinting are potential candidates. For materials like graphene, which are deposited using CVD on particular substrate (Cu and Ni foils), it will be crucial

to develop R2R transfer technologies while minimizing the transfer damage on the quality of those TCE materials.

## Conclusions

To accelerate the commercialization of f-PSCs, the development of f-TCEs with exceptionally high conductivity, environmental stability, and cost-effective production technologies is imperative. Various f-TCEs developed recently were reviewed and their performances were compared with respect to optical, electrical and mechanical properties depending on different materials and designs that they used. Future challenges and prospects towards commercialization were also discussed. Progress in embedding metal mesh-based TCEs within substrates, along with the exploration of novel high-performance TCE materials, is essential to minimize resistive losses and enable modularization-free large-area PSCs. Additionally, the advancement of flexible encapsulation techniques, such as thin film encapsulation (TFE) utilizing alternating organic and inorganic layers, will significantly enhance resistance to moisture and oxygen. Finally, the realization of these components through scalable and cost-effective production technologies is crucial for their successful integration into commercial products.

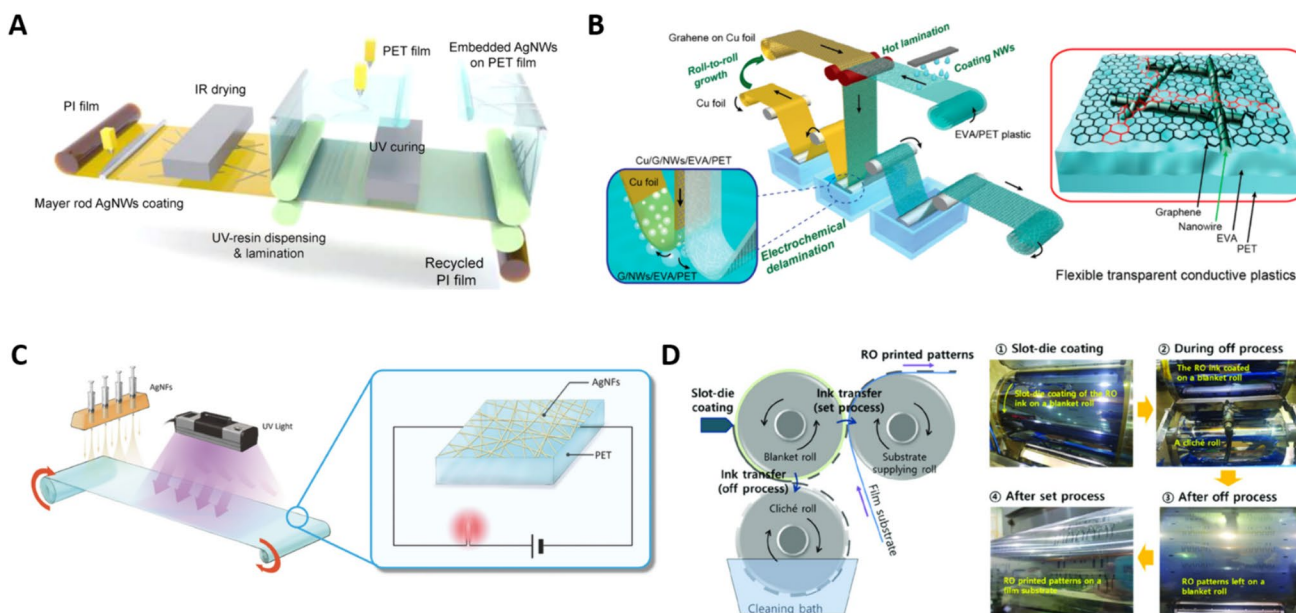


**Fig. 8** Promising technologies for R2R method of f-TCEs. **A** Schematic of the R2R process for fabricating embedded Ag-nanowire electrodes via the Mayer rod coating method. Reproduced with permission from [102]. Copyright 2017, Elsevier. **B** Schematic of the R2R process for producing graphene and Ag-nanowire hybrid films via CVD and hot lamination. Reprinted with permission from [103]. Copyright 2015, American Chemical Society. **C** Schematic

of the R2R fabrication of AgNF networks, including blow spinning and simultaneous UV irradiation. Reproduced with permission from [104]. Copyright 2017, John Wiley and Sons. **D** Schematic of the R2R continuous reverse-offset printing process for mesh electrodes using Ag NP ink via slot-die coating. Reproduced with permission from [105]. Copyright 2020, John Wiley and Sons

**Acknowledgements** This research was supported by the Challengeable Future Defense Technology Research and Development Program through the Agency For Defense Development (ADD) funded by the Defense Acquisition Program Administration (DAPA) in 2024(No.912765601).

**Data availability** All data are available in the main text. Further data are available from the corresponding author on reasonable request.

## References

- M.A. Green, A. Ho-Baillie, H.J. Snaith, *Nat. Photonics* **8**, 506 (2014)
- G.E. Eperon, S.D. Stranks, C. Menelaou, M.B. Johnston, L.M. Herz, H.J. Snaith, *Energy Environ. Sci.* **7**, 982 (2014)
- S.D. Stranks, G.E. Eperon, G. Grancini, C. Menelaou, M.J.P. Alcocer, T. Leijtens, L.M. Herz, A. Petrozza, H.J. Snaith, *Science* **342**, 341 (2013)
- Q. Dong, Y. Fang, Y. Shao, P. Mulligan, J. Qiu, L. Cao, J. Huang, *Science* **347**, 967 (2015)
- NREL best research-cell efficiency chart. <https://www.nrel.gov/pv/cell-efficiency.html> Accessed 29 July 2024
- J. You, Z. Hong, Y.M. Yang, Q. Chen, M. Cai, T.-B. Song, C.-C. Chen, S. Lu, Y. Liu, H. Zhou, Y. Yang, *ACS Nano* **8**, 1674 (2014)
- Q. Wang, Y. Shao, Q. Dong, Z. Xiao, Y. Yuan, J. Huang, *Energy Environ. Sci.* **7**, 2359 (2014)
- W. Ke, G. Fang, Q. Liu, L. Xiong, P. Qin, H. Tao, J. Wang, H. Lei, B. Li, J. Wan, G. Yang, Y. Yan, *J. Am. Chem. Soc.* **137**, 6730 (2015)
- Z. Li, T.R. Klein, D.H. Kim, M. Yang, J.J. Berry, M.F.A.M. van Hest, K. Zhu, *Nat. Rev. Mater.* **3**, 1 (2018)
- K. Hwang, Y.S. Jung, Y.J. Heo, F.H. Scholes, S.E. Watkins, J. Subbiah, D.J. Jones, D.Y. Kim, D. Vak, *Adv. Mater.* **27**, 1241 (2015)
- B. Dou, J.B. Whitaker, K. Bruening, D.T. Moore, L.M. Wheeler, J. Ryter, N.J. Breslin, J.J. Berry, S.M. Garner, F.S. Barnes, S.E. Shaheen, C.J. Tassone, K. Zhu, M.F.A.M. van Hest, *ACS Energy Lett.* **3**, 2558 (2018)
- B. Hailegnaw, S. Demchyshyn, C. Putz, L.E. Lehner, F. Mayr, D. Schiller, R. Pruckner, M. Cobet, D. Ziss, T.M. Krieger, A. Rastelli, N.S. Sariciftci, M.C. Scharber, M. Kaltenbrunner, *Nat. Energy* **9**, 677 (2024)
- N. Ren, L. Tan, M. Li, J. Zhou, Y. Ye, B. Jiao, L. Ding, C. Yi, *iEnergy* **3**, 39 (2024)
- U. Kim, M. Han, J. Jang, J. Shin, M. Park, J. Byeon, M. Choi, *Adv. Energy Mater.* **13**, 2203198 (2022)
- G. Lee, M.-C. Kim, Y.W. Choi, N. Ahn, J. Jang, J. Yoon, S.M. Kim, J.-G. Lee, D. Kang, H.S. Jung, M. Choi, *Energy Environ. Sci.* **12**, 3182 (2019)
- K. Zhu, Z. Lu, S. Cong, G. Cheng, P. Ma, Y. Lou, J. Ding, N. Yuan, M.H. Rummeli, G. Zou, *Small* **15**, 1902878 (2019)
- X. Hu, Z. Huang, F. Li, M. Su, Z. Huang, Z. Zhao, Z. Cai, X. Yang, X. Meng, P. Li, Y. Wang, M. Li, Y. Chen, Y. Song, *Energy Environ. Sci.* **12**, 979 (2019)
- N.T. Jafferis, E.F. Helbling, M. Karpelson, R.J. Wood, *Nature* **570**, 491 (2019)
- G.M. Paternò, V. Robbiano, L. Santarelli, A. Zampetti, C. Cazaniga, V. García Sakai, F. Cacialli, *Sustain. Energy Fuels* **3**, 2561 (2019)
- A.G. Boldyreva, A.F. Akbulatov, S.A. Tsarev, S.Y. Luchkin, I.S. Zhidkov, E.Z. Kurmaev, K.J. Stevenson, V.G. Petrov, P.A. Troshin, *J. Phys. Chem. Lett.* **10**, 813 (2019)
- D. Pérez-del-Rey, C. Dreessen, A.M. Igual-Muñoz, L. van den Hengel, M.C. Gélvez-Rueda, T.J. Savenije, F.C. Grozema, C. Zimmermann, H.J. Bolink, *Sol. RRL* **4**, 2000447 (2020)
- K. Huang, K. Yang, H. Li, S. Zheng, J. Wang, H. Guo, Y. Peng, X. Zhong, J. Yang, A.C.S. Appl. Energy Mater. **3**, 7318 (2020)
- T.M. Koh, H. Wang, Y.F. Ng, A. Bruno, S. Mhaisalkar, N. Mathews, *Adv. Mater.* **34**, 2104661 (2022)
- D. Yang, R. Yang, S. Priya, S.F. Liu, *Angew. Chem. Int. Ed.* **58**, 4466 (2019)
- C. Teixeira, P. Spinelli, L.A. Castriotta, D. Müller, S. Öz, L. Andrade, A. Mendes, A.D. Carlo, U. Würfel, K. Wojciechowski, D. Forgács, *Adv. Funct. Mater.* **32**, 2206761 (2022)
- D.R. Cairns, R.P. Witte, D.K. Sparacin, S.M. Sachsman, D.C. Paine, G.P. Crawford, R.R. Newton, *Appl. Phys. Lett.* **76**, 1425 (2000)
- Y. Leterrier, L. Médico, F. Demarco, J.A.E. Manson, U. Betz, M.F. Escolà, M. Kharrazi Olsson, F. Atamny, *Thin Solid Films* **460**, 156 (2004)
- K. Sun, P. Li, Y. Xia, J. Chang, J. Ouyang, A.C.S. Appl. Mater. Interfaces **7**, 15314 (2015)
- M. Dianetti, F. Di Giacomo, G. Polino, C. Ciceroni, A. Liscio, A. D'Epifanio, S. Licoccia, T.M. Brown, A. Di Carlo, F. Brunetti, *Sol. Energy Mater. Sol. Cells* **140**, 150 (2015)
- X. Hu, X. Meng, X. Yang, Z. Huang, Z. Xing, P. Li, L. Tan, M. Su, F. Li, Y. Chen, Y. Song, *Sci. Bull.* **66**, 527 (2021)
- E. Lee, J. Ahn, H.C. Kwon, S. Ma, K. Kim, S. Yun, J. Moon, *Adv. Energy Mater.* **8**, 1702182 (2017)
- H.-G. Im, S. Jeong, J. Jin, J. Lee, D.-Y. Youn, W.-T. Koo, S.-B. Kang, H.-J. Kim, J. Jang, D. Lee, H.-K. Kim, I.-D. Kim, J.-Y. Lee, B.-S. Bae, *NPG Asia Mater.* **8**, e282 (2016)
- H. Yang, H.C. Kwon, S. Ma, K. Kim, S.C. Yun, G. Jang, J. Park, H. Lee, S. Goh, J. Moon, *A.C.S. Appl. Mater. Interfaces* **12**, 13824 (2020)
- M. Li, W.W. Zuo, A.G. Ricciardulli, Y.G. Yang, Y.H. Liu, Q. Wang, K.L. Wang, G.X. Li, M. Saliba, D. Di Girolamo, A. Abate, Z.K. Wang, *Adv. Mater.* **32**, 2003422 (2020)
- H. Ji, J. Huang, W. Zhang, X. Chen, Y. Lu, C. Ding, J. Fang, W. Song, L. Ai, *Adv. Mater. Interf* **9**, 2200483 (2022)
- Y. Yang, F. Min, Y. Qiao, Z. Li, F. Vogelbacher, Z. Liu, W. Lv, Y. Wang, Y. Song, *Nano Energy* **89**, 106384 (2021)
- Z. Liu, P. You, C. Xie, G. Tang, F. Yan, *Nano Energy* **28**, 151 (2016)
- S. Kim, H.S. Lee, J.M. Kim, S.W. Seo, J.H. Kim, C.W. Jang, S.-H. Choi, *J. Alloys Compd.* **744**, 404 (2018)
- J. Yoon, H. Sung, G. Lee, W. Cho, N. Ahn, H.S. Jung, M. Choi, *Energy Environ. Sci.* **10**, 337 (2017)
- X. Xu, H. Wang, J. Wang, M. Muhammad, Z. Wang, P. Chen, W. Zhao, B. Kang, J. Zhang, C. Li, Y. Duan, *A.C.S. Appl. Energy Mater.* **3**, 4208 (2020)
- W. Chen, R. Zhang, X. Yang, H. Wang, H. Yang, X. Hu, S. Zhang, *J. Mater. Chem. C* **10**, 8625 (2022)
- A.I. Hofmann, E. Cloutet, G. Hadziioannou, *Adv. Electron. Mater.* **4**, 1700412 (2018)
- J. Schneider, P. Rohner, D. Thureja, M. Schmid, P. Galliker, D. Poulidakos, *Adv. Funct. Mater.* **26**, 833 (2015)
- H.B. Lee, W.-Y. Jin, M.M. Ovhall, N. Kumar, J.-W. Kang, *J. Mater. Chem. C* **7**, 1087 (2019)
- A. Anand, M.M. Islam, R. Meitzner, U.S. Schubert, H. Hoppe, *Adv. Energy Mater.* **11**, 2100875 (2021)
- D.B. Fraser, H.D. Cook, *J. Electrochem. Soc.* **119**, 1368 (1972)
- G. Haacke, *J. Appl. Phys.* **47**, 4086 (1976)
- M. Dressel, G. Grüner, *Electrodynamics of solids* (Cambridge University Press, London, 2002)
- J.A. Mendez-Gamboa, R. Castro-Rodriguez, I.V. Perez-Quintana, R.A. Medina-Esquivel, A. Martel-Arbelo, *Thin Solid Films* **599**, 14 (2016)

50. I.R. Cisneros-Contreras, A.L. Muñoz-Rosas, A. Rodríguez-Gómez, *Results Phys.* **15**, 102695 (2019)
51. C. Peng, Z. Jia, H. Neilson, T. Li, J. Lou, *Adv. Eng. Mater.* **15**, 250 (2012)
52. L.D. Landau, E.M. Lifshitz, *Theory of elasticity*, 3rd edn. (Butterworth-Heinemann, NY, 1986), p.42
53. H. Wang, Z. Huang, S. Xiao, X. Meng, Z. Xing, L. Rao, C. Gong, R. Wu, T. Hu, L. Tan, X. Hu, S. Zhang, Y. Chen, *J. Mater. Chem. A* **9**, 5759 (2021)
54. Z. Li, K. Cao, J. Li, X. Du, Y. Tang, B. Yu, *Org. Electron.* **81**, 105675 (2020)
55. U. Kim, J.S. Nam, J. Yoon, J. Han, M. Choi, I. Jeon, *Carbon Energy* **6**, e471 (2024)
56. X. Meng, Z. Cai, Y. Zhang, X. Hu, Z. Xing, Z. Huang, Z. Huang, Y. Cui, T. Hu, M. Su, X. Liao, L. Zhang, F. Wang, Y. Song, Y. Chen, *Nat. Commun.* **11**, 3016 (2020)
57. M.W. Rowell, M.D. McGehee, *Energy Environ. Sci.* **4**, 131 (2011)
58. Y. Yang, H. Deng, Q. Fu, *Mater. Chem. Front.* **4**, 3130 (2020)
59. B.J. Worfolk, S.C. Andrews, S. Park, J. Reinspach, N. Liu, M.F. Toney, S.C. Mannsfeld, Z. Bao, *Proc. Natl. Acad. Sci. U.S.A.* **112**, 14138 (2015)
60. B. Vaagensmith, K.M. Reza, M.N. Hasan, H. Elbohy, N. Adhikari, A. Dubey, N. Kantack, E. Gaml, Q. Qiao, A.C.S. Appl. Mater. Interfaces **9**, 35861 (2017)
61. S.I. Na, S.S. Kim, J. Jo, D.Y. Kim, *Adv. Mater.* **20**, 4061 (2008)
62. N. Kim, S. Kee, S.H. Lee, B.H. Lee, Y.H. Kahng, Y.R. Jo, B.J. Kim, K. Lee, *Adv. Mater.* **26**, 2268 (2014)
63. N. Kim, H. Kang, J.H. Lee, S. Kee, S.H. Lee, K. Lee, *Adv. Mater.* **27**, 2317 (2015)
64. C. Yeon, S.J. Yun, J. Kim, J.W. Lim, *Adv. Electron. Mater.* **1**, 1500121 (2015)
65. C. Badre, L. Marquant, A.M. Alsayed, L.A. Hough, *Adv. Funct. Mater.* **22**, 2723 (2012)
66. Y. Wang, C. Zhu, R. Pfattner, H. Yan, L. Jin, S. Chen, F. Molina-Lopez, F. Lissel, J. Liu, N.I. Rabiah, Z. Chen, J.W. Chung, C. Linder, M.F. Toney, B. Murmann, Z. Bao, *Sci. Adv.* **3**, e1602076 (2017)
67. Y. Galagan, E.W.C. Coenen, S. Sabik, H.H. Gorter, M. Barink, S.C. Veenstra, J.M. Kroon, R. Andriessen, P.W.M. Blom, *Sol. Energy Mater. Sol. Cells* **104**, 32 (2012)
68. Z. Zhong, P. Ko, H. Youn, A. Kim, K. Woo, *Int. J. Precis. Eng. Manuf. Green Technol.* **8**, 1711 (2021)
69. R. Miao, P. Li, W. Zhang, X. Feng, L. Qian, J. Fang, W. Song, W. Wang, *Adv. Interf. Mater.* (2021). <https://doi.org/10.1002/admi.202101669>
70. J. Gong, X. Fan, Z. Zong, M. Yang, Y. Sun, G. Zhao, *RSC Adv.* **13**, 15531 (2023)
71. Y. Wang, G.J. Weng, in *Electrical Conductivity of Carbon Nanotube- and Graphene -Based Nanocomposites*, in *Micromechanics and Nanomechanics of Composite Solids*. ed. by S.A. Meguid, G.J. Weng (Springer, Cham, 2018), pp.123–156
72. R. Okuda, K. Niwano, K. Hatada, K. Kokubu, R. Suga, T. Watanabe, S. Koh, *Sci. Rep.* **13**, 13878 (2023)
73. D.A. Ilatovskii, E.P. Gilshtein, O.E. Glukhova, A.G. Nasibulin, *Adv. Sci.* **9**, 2201673 (2022)
74. K. Cao, S. Feng, Y. Han, L. Gao, T. Hue Ly, Z. Xu, Y. Lu, *Nat. Commun.* **11**, 284 (2020)
75. Y. Bai, R. Zhang, X. Ye, Z. Zhu, H. Xie, B. Shen, D. Cai, B. Liu, C. Zhang, Z. Jia, S. Zhang, X. Li, F. Wei, *Nat. Nanotechnol.* **13**, 589 (2018)
76. I. Jeon, T. Chiba, C. Delacou, Y. Guo, A. Kaskela, O. Reynaud, E.I. Kauppinen, S. Maruyama, Y. Matsuo, *Nano Lett.* **15**, 6665 (2015)
77. I. Jeon, J. Yoon, U. Kim, C. Lee, R. Xiang, A. Shawky, J. Xi, J. Byeon, H.M. Lee, M. Choi, S. Maruyama, Y. Matsuo, *Adv. Energy Mater.* **9**, 1901204 (2019)
78. J.H. Heo, D.H. Shin, S. Kim, M.H. Jang, M.H. Lee, S.W. Seo, S.-H. Choi, S.H. Im, *Chem. Eng. J.* **323**, 153 (2017)
79. J. Yoon, U. Kim, Y. Yoo, J. Byeon, S.K. Lee, J.S. Nam, K. Kim, Q. Zhang, E.I. Kauppinen, S. Maruyama, P. Lee, I. Jeon, *Adv. Sci.* **8**, 2004092 (2021)
80. J.H. Heo, D.H. Shin, M.L. Lee, M.G. Kang, S.H. Im, A.C.S. Appl. Mater. Interfaces **10**, 31413 (2018)
81. I. Jeon, J. Yoon, N. Ahn, M. Atwa, C. Delacou, A. Anisimov, E.I. Kauppinen, M. Choi, S. Maruyama, Y. Matsuo, *J. Phys. Chem. Lett.* **8**, 5395 (2017)
82. B. Dou, E.M. Miller, J.A. Christians, E.M. Sanehira, T.R. Klein, F.S. Barnes, S.E. Shaheen, S.M. Garner, S. Ghosh, A. Mallick, D. Basak, M. van Hest, *J. Phys. Chem. Lett.* **8**, 4960 (2017)
83. J. Chung, S.S. Shin, K. Hwang, G. Kim, K.W. Kim, D.S. Lee, W. Kim, B.S. Ma, Y.-K. Kim, T.-S. Kim, J. Seo, *Energy Environ. Sci.* **13**, 4854 (2020)
84. L. Yang, J. Feng, Z. Liu, Y. Duan, S. Zhan, S. Yang, K. He, Y. Li, Y. Zhou, N. Yuan, J. Ding, S.F. Liu, *Adv. Mater.* **34**, 2201681 (2022)
85. D. Yang, R. Yang, C. Zhang, T. Ye, K. Wang, Y. Hou, L. Zheng, S. Priya, S.F. Liu, *Adv. Mater.* **35**, 2302484 (2023)
86. T. Xue, B. Fan, K.-J. Jiang, Q. Guo, X. Hu, M. Su, E. Zhou, Y. Song, *Energy Environ. Sci.* **17**, 2621 (2024)
87. Z. Li, C. Jia, Z. Wan, J. Xue, J. Cao, M. Zhang, C. Li, J. Shen, C. Zhang, Z. Li, *Nat. Commun.* **14**, 6451 (2023)
88. M. Li, J. Zhou, L. Tan, H. Li, Y. Liu, C. Jiang, Y. Ye, L. Ding, W. Tress, C. Yi, *The Innovation* **3**, 100310 (2022)
89. Y. Wang, Y. Meng, C. Liu, R. Cao, B. Han, L. Xie, R. Tian, X. Lu, Z. Song, J. Li, S. Yang, C. Lu, Z. Ge, *Joule* **8**, 1120 (2024)
90. N. Ohashi, R. Kaneko, C. Sakai, Y. Wasai, S. Higuchi, K. Yazawa, H. Tahara, T. Handa, T. Nakamura, R. Murdey, Y. Kanemitsu, A. Wakamiya, *Sol. RRL* **7**, 2300221 (2023)
91. S. Ahn, T.H. Han, K. Maleski, J. Song, Y.H. Kim, M.H. Park, H. Zhou, S. Yoo, Y. Gogotsi, T.W. Lee, *Adv. Mater.* **32**, 2000919 (2020)
92. H. Zhou, S.J. Han, H.D. Lee, D. Zhang, M. Anayee, S.H. Jo, Y. Gogotsi, T.W. Lee, *Adv. Mater.* **34**, 2206377 (2022)
93. L. Gao, L. Chao, M. Hou, J. Liang, Y. Chen, H.-D. Yu, W. Huang, *Npj Flex. Electron.* **3**, 4 (2019)
94. H. Li, X. Li, W. Wang, J. Huang, J. Li, Y. Lu, J. Chang, J. Fang, W. Song, *Sol. RRL* **3**, 1800317 (2019)
95. C. Gao, S. Yuan, K. Cui, Z. Qiu, S. Ge, B. Cao, J. Yu, *Sol. RRL* **2**, 1800175 (2018)
96. P. Ma, Y. Lou, S. Cong, Z. Lu, K. Zhu, J. Zhao, G. Zou, *Adv. Energy Mater.* **10**, 1903357 (2020)
97. L. Li, P. Chen, R. Su, H. Xu, Q. Li, Q. Zhong, H. Yan, X. Yang, J. Hu, S. Li, T. Huang, Y. Xiao, B. Liu, Y. Ji, D. Wang, H. Sun, X. Guo, Z.H. Lu, H.J. Snaith, Q. Gong, L. Zhao, R. Zhu, *Adv. Mater.* **36**, 2305238 (2024)
98. W. Jung, Y.-H. Jung, P.V. Pikhitsa, J. Feng, Y. Yang, M. Kim, H.-Y. Tsai, J. Shin, K.-Y. Kim, H. Choi, J. Rho, M. Choi, *Nature* **592**(7852), 54 (2021)
99. J. Shin, Y.-H. Jung, P.V. Pikhitsa, C. Hur, W. Cho, W. Jung, M. Choi, *Addit. Manuf.* **60**, 103206 (2022)
100. S. Zips, B. Huang, S. Hotte, L. Hiendlmeier, C. Wang, K. Rajamani, O. Buriez, G. Al Boustani, Y. Chen, B. Wolfrum, A. Yamada, *ACS. Appl. Mater. Interf.* **15**, 35950 (2023)
101. X. Chen, S. Nie, W. Guo, F. Fei, W. Su, W. Gu, Z. Cui, *Adv. Electron. Mater.* **5**, 1800991 (2019)
102. E. Jung, C. Kim, M. Kim, H. Chae, J.H. Cho, S.M. Cho, *Org. Electron.* **41**, 190 (2017)

103. B. Deng, P.C. Hsu, G. Chen, B.N. Chandrashekar, L. Liao, Z. Ayitimuda, J. Wu, Y. Guo, L. Lin, Y. Zhou, M. Aisijiang, Q. Xie, Y. Cui, Z. Liu, H. Peng, *Nano Lett.* **15**, 4206 (2015)
104. S. Lin, X. Bai, H. Wang, H. Wang, J. Song, K. Huang, C. Wang, N. Wang, B. Li, M. Lei, H. Wu, *Adv. Mater.* **29**, 1703238 (2017)
105. Z. Zhong, P. Ko, J.Y. Seok, H. Kim, S. Kwon, H. Youn, K. Woo, *Adv. Eng. Mater.* **22**, 2000463 (2020)

Springer Nature or its licensor (e.g. a society or other partner) holds exclusive rights to this article under a publishing agreement with the author(s) or other rightsholder(s); author self-archiving of the accepted manuscript version of this article is solely governed by the terms of such publishing agreement and applicable law.

**Publisher's Note** Springer Nature remains neutral with regard to jurisdictional claims in published maps and institutional affiliations.